

# Morphodynamics of barchan-barchan interactions investigated at the grain scale

An edited version of this paper was published by AGU. Copyright (2021) American Geophysical Union. Assis, W. R. and Franklin, E. M. (2021). Morphodynamics of barchan-barchan interactions investigated at the grain scale. *Journal of Geophysical Research: Earth Surface*, 126, e2021JF006237. <https://doi.org/10.1029/2021JF006237>.

To view the published open abstract, go to <https://doi.org/10.1029/2021JF006237>.

**W. R. Assis<sup>1</sup>, E. M. Franklin<sup>1</sup>**

<sup>1</sup>School of Mechanical Engineering, UNICAMP - University of Campinas,  
Rua Mendeleev, 200, Campinas, SP, Brazil

## Key Points:

- We determine the trajectories of individual grains during barchan-barchan interactions
- We show the origin and destination of moving grains and typical lengths and velocities
- We find the spreading rate of grains over the target barchan once dune-dune collision has occurred

---

Corresponding author: Erick M. Franklin, [erick.franklin@unicamp.br](mailto:erick.franklin@unicamp.br)

**Abstract**

Corridors of size-selected crescent-shaped dunes, known as barchans, are commonly found in water, air, and other planetary environments. The growth of barchans results from the interplay between a fluid flow and a granular bed, but their size regulation involves intricate exchanges between different barchans within a field. One size-regulating mechanism is the binary interaction between nearby dunes, when two dunes exchange mass via the near flow field or by direct contact (collision). In a recent Letter (Assis & Franklin, 2020), we identified five different patterns arising from binary interactions of subaqueous barchans, and proposed classification maps. In this paper, we further inquire into binary exchanges by investigating the motion of individual grains while barchans interact with each other. The experiments were conducted in a water channel where the evolution of pairs of barchans in both aligned and off-centered configurations was recorded by conventional and high-speed cameras. Based on image processing, we obtained the morphology of dunes and motion of grains for all interaction patterns. We present the trajectories of individual grains, from which we show the origin and destination of moving grains, and their typical lengths and velocities. We also show that grains from the impacting dune spread with a diffusion-like component over the target barchan, and we propose a diffusion length. Our results provide new insights into the size-regulating mechanisms of barchans and barchanoid forms found on Earth and other planets.

**Plain Language Summary**

Barchans are dunes of crescentic shape that are commonly found on Earth, Mars and other celestial bodies. Although of similar shape, their scales vary with the environment they are in, going from the millennium and kilometer for Martian barchans, down to the minute and centimeter in the aquatic case, passing by hundreds of meters and years for aeolian barchans. Other common characteristic is that barchans are organized in dune fields, where barchan-barchan collisions are an important mechanism for their size regulation. We took advantage of the smaller and faster scales of subaqueous dunes and performed experiments in a water channel, which allowed us to determine the trajectories of individual grains while two barchans interacted with each other, something unfeasible from field measurements on terrestrial or Martian deserts. We show typical lengths and velocities of individual grains, and that, in case of barchan collisions, grains from the impacting barchan spread with a diffusive component over the other barchan. Our results provide new insights into the evolution of barchans found in water, air, and other planetary environments.

**1 Introduction**

Fields of barchan dunes, crescent-shaped dunes with horns pointing downstream, are commonly found in different environments, such as rivers, Earth's deserts and on the surface of Mars (Bagnold, 1941; Herrmann & Sauermann, 2000; Hersen, 2004; Elbelrhiti et al., 2005; Claudin & Andreotti, 2006; E. J. R. Parteli & Herrmann, 2007), being characterized by corridors of size-selected barchans. The growth of dunes results from the interplay between a fluid flow and a granular bed, with sand being transported as a moving layer called bedload. Barchan dunes usually appear under a one-directional fluid flow and limited sand supply (Bagnold, 1941), but the regulation of their size involves intricate interactions between different barchans within a field (Hersen et al., 2004; Hersen & Douady, 2005; Kocurek et al., 2010; Génois, Hersen, et al., 2013; Génois, du Pont, et al., 2013). Barchan fields observed in nature result thus from complex interactions between a fluid flow, a sand bed, and existing bedforms.

Hersen et al. (2004) showed that an isolated barchan within a dune field is marginally stable, since it receives and loses sand in proportion to its width and size of horns, respectively, meaning that the net flux of sand is positive for large barchans and negative

68 for small ones. In addition, because smaller dunes move faster than larger ones (Bagnold,  
69 1941), collisions could lead to a coarsening of the barchan field. Elbelrhiti et al. (2005)  
70 showed that, in fact, barchan-barchan collisions and changes in wind direction induce  
71 surface waves that propagate faster than the barchan itself, which can regulate the size  
72 of barchans. If the barchan dune is larger than the characteristic length of the surface  
73 waves, the latter propagate toward one of the barchan horns and new barchans are ejected,  
74 a mechanism known as calving. Otherwise, calving is not observed (in case of a barchan-  
75 barchan collision, the two barchans simply merge). Later, Worman et al. (2013) proposed  
76 that the wake of an upstream barchan can lead to calving on a downstream dune prior  
77 (or even without) a barchan-barchan collision, due to the same wave mechanism shown  
78 by Elbelrhiti et al. (2005).

79 The first studies on barchan interactions were based on field measurements of ae-  
80 lian barchans, such as done by Norris and Norris (1961) and Gay (1999). Field mea-  
81 surements are still important in investigating barchan interactions (Vermeesch, 2011; El-  
82 belrhiti et al., 2008; Hugenholtz & Barchyn, 2012), having shown that size regulation and  
83 the appearance of barchanoid forms are highly influenced by barchan-barchan collisions.  
84 However, given the long timescales in the aeolian case (of the order of the decade), time  
85 series for barchan collisions in aeolian fields are frequently incomplete, and conclusive  
86 results would need around a century to be achieved. In order to overcome this problem,  
87 numerical and experimental investigations were carried out over the last decades.

88 The numerical investigations were conducted using simplified models, both con-  
89 tinuum (Schwämmle & Herrmann, 2003; Durán et al., 2005; Zhou et al., 2019) and dis-  
90 crete (Katsuki et al., 2011), and most of them incorporated a few rules of barchan in-  
91 teractions in order to inquire into the mechanisms of sand distribution and evolution of  
92 dune fields. In particular, Lima et al. (2002) and E. Parteli and Herrmann (2003) pro-  
93 posed a simple model based on the inter-dune sand flux and a rule for the merging (co-  
94 alescence) of dunes, Lima et al. (2002) investigating barchan dunes in two dimensions  
95 and E. Parteli and Herrmann (2003) transverse dunes in one dimension. As results, Lima  
96 et al. (2002) showed that barchans reach eventually comparable sizes and are confined  
97 to corridors, and E. Parteli and Herrmann (2003) that transverse dunes reach both the  
98 same heights and velocities. Later, Katsuki et al. (2005) and Durán et al. (2009) carried  
99 out numerical simulations to investigate the outcome of barchan-barchan collisions, from  
100 which they obtained the merging and exchange patterns (described in what follows). In  
101 addition, Durán et al. (2009) proposed an equation for the size distribution of barchans  
102 based on a balance of sand flux and a collision model. In the same line of Durán et al.  
103 (2009), Génois, du Pont, et al. (2013) proposed an agent-based model using the balance  
104 of sand fluxes and elementary rules for barchan-barchan collisions that included a fragmentation-  
105 exchange pattern (described next) in addition to the merging and exchange ones. As gen-  
106 eral results, the models of Durán et al. (2009) and Génois, du Pont, et al. (2013) found  
107 that sand distribution due to collisions is a mechanism that explains the existence of cor-  
108 ridors of size-selected barchans, with sparse and large or dense and small barchans. Dif-  
109 ferent from previous works, Bo and Zheng (2013) simulated numerically the growth and  
110 evolution of a barchan field using a scale-coupled model (Zheng et al., 2009) in order to  
111 obtain the probability of barchan-barchan collisions. They found the probabilities for  
112 the occurrence of three collision patterns (merging, exchange and fragmentation-exchange,  
113 described next), and showed that probabilities vary with the flow strength, grain diam-  
114 eter, grain supply and height ratio of barchans. However, although varying several pa-  
115 rameters, the authors did not investigate the mechanics of collisions, which remains to  
116 be fully understood.

117 In common, previous numerical works pointed toward homogeneous fields, but, al-  
118 though those investigations reproduced some collision types, model simplifications pre-  
119 vented them from reproducing correctly all existing short-range interactions (including  
120 collisions). Being more specific, the interactions strongly influenced by wake effects (chas-

ing and fragmentation-chasing, described next), for which collision does not occur, are not explicitly dealt with, and the effects of grain types and flow conditions are not taken into account. Besides, numerical studies at the grain scale, showing the trajectories of individual grains, do not exist at the moment. Some of these aspects were only investigated recently (experimentally) at the bedform scale (Assis & Franklin, 2020), and there is a complete lack of information at the grain scale.

Given the relatively fast and small scales of the subaqueous case (in the order of minutes and centimeters), the experiments on barchan-barchan interactions were conducted in water tanks and channels (with the exception of Palmer et al. (2012)). Part of them investigated the disturbances in the fluid flow as two barchans approach each other, which may affect greatly bedload and surface erosion. In a sequence of experimental works, Palmer et al. (2012) investigated the flow disturbances caused by an upstream barchan upon a downstream one in a wind tunnel when they are in an aligned configuration, for which they varied the volume ratios and fixed the longitudinal separation, and Bristow et al. (2018), Bristow et al. (2019) and Bristow et al. (2020) investigated the off-centered configuration in a water channel, where they fixed the volume ratio and varied the longitudinal separations. The experiments made use of particle image velocimetry (PIV), and found that the wake of the upstream dune increases turbulence levels on the downstream stoss surface, causing thus a larger erosion on the downstream dune, and that the transverse offset creates a channeling effect around one of the horns of the downstream barchan, promoting dune asymmetry. They showed also that near-bed fluctuations are particularly increased at the reattachment point and that streamwise vortices emerge from the horns, which can enhance even more erosion on the downstream barchan depending on the relative positions of dunes.

Another part of experiments were concerned with the bedform evolution as two dunes interacted with each other. In particular, Endo et al. (2004) and Hersen and Douady (2005) investigated barchan-barchan collisions, the former using a water flume to study the collisions of aligned barchans and the latter a tank in which the motion of a tray created a relative flow between the water and the bedform to investigate the collisions of off-centered barchans. While Endo et al. (2004) varied the mass ratio of barchans and kept the water flow rate, initial conditions and grain types fixed, Hersen and Douady (2005) varied the transverse distance of colliding dunes (referred to as impact or offset parameter) and maintained the other parameters fixed. In this way, these works complemented each other to a certain extent and showed, as main results, that barchan-barchan collisions produce smaller dunes, promoting sand redistribution. In addition, Endo et al. (2004) identified three types of collision patterns, which they named absorption, ejection and split, and which we call merging, exchange and fragmentation-chasing (Assis & Franklin, 2020) and explain in what follows. For other kinds of dunes, Bacik et al. (2020) investigated the interaction between a pair of two-dimensional dunes in a narrow Couette-type circular channel, where, under the action of a turbulent flow, the pair of dunes interacted with each other over long times. Under such spanwise confinement, they found that turbulent structures of the flow induce a dune-dune repulsion that prevents dune collisions. They conjectured that such mechanism could happen for the interaction of two barchans of comparable size.

In spite of all those findings, a general picture for all barchan-barchan interactions was still lacking, i.e., the identification and organization of all interaction patterns in a parameter space including all relevant parameters: initial separation and alignment, dune masses, grain properties, and fluid velocity. In a recent paper (Assis & Franklin, 2020), we investigated experimentally the short-range binary interactions of subaqueous barchans, including collisions, in both aligned and off-centered configurations. The experiments were conducted in a transparent channel where controlled grains were entrained by the water flow, forming a pair of barchans that interacted with each other. We varied the water flow rates, grain types (diameter, density and roundness), pile masses, longitudinal

174 and transverse distances, and initial conditions. As a result, we identified five interac-  
 175 tion patterns for both aligned and off-centered configurations and proposed two maps  
 176 that provide a comprehensive classification for barchan-barchan interactions based on  
 177 the ratio between the number of grains of each dune, Shields number and alignment of  
 178 barchans. The five different patterns observed were classified as (i) chasing, when the  
 179 upstream barchan does not reach the downstream one; (ii) merging, when the upstream  
 180 barchan reaches the downstream one and they merge; (iii) exchange, when, once the up-  
 181 stream barchan reaches the downstream one, a small barchan is ejected; (iv) fragmentation-  
 182 chasing, when the downstream dune splits before being reached by the upstream barchan  
 183 and the new dunes outrun the upstream one; and (v) fragmentation-exchange, when frag-  
 184 mentation initiates, the upstream barchan reaches the splitting dune, and, once they touch,  
 185 a small barchan is ejected. In addition, we showed that an ejected barchan has roughly  
 186 the same mass of the impacting one and that the asymmetry of the downstream barchan  
 187 is larger in wake-dominated processes. However, details at the grain scale of barchan-  
 188 barchan interactions were not investigated.

189 Although previous studies have shown that barchan-barchan collision can be a size-  
 190 regulating mechanism and identified the interaction patterns, none of them investigated  
 191 the mass transfers between barchans prior and during collisions, the motion of grains once  
 192 collision took place, nor, with the exception, partially, of Assis and Franklin (2020), the  
 193 dune morphodynamics during collisions. Therefore, mass transfers and motions at the  
 194 grain scale during barchan-barchan interactions remain completely unknown. In this pa-  
 195 per, we further inquire into barchan-barchan interactions by investigating the motion of  
 196 grains while barchans interact with each other, allowing us to compute the mass exchanged  
 197 between barchans and lost by the system, and the spreading of grains of an impacting  
 198 barchan over the target one. The experiments were conducted in a water channel where  
 199 the evolution of pairs of barchans in both aligned and off-centered configurations was recorded  
 200 by conventional and high-speed cameras. Based on image processing, we tracked bed-  
 201 forms and grains for all interaction patterns. We present the trajectories of individual  
 202 grains during different stages of barchan-barchan interactions, from which we find the  
 203 origin and destination of moving grains, their typical lengths and velocities, and the pro-  
 204 portions of grains exchanged between barchans and lost by the entire system. We also  
 205 show that grains from the impacting dune spread with a diffusion-like component over  
 206 the target barchan, and propose a diffusion length for their dispersion. The present re-  
 207 sults provide new insights into the shape and size variations of barchans and barchanoid  
 208 forms found in water, air, and other planetary environments.

209 In the following, Sec. 2 describes the experimental setup and procedure, Sec. 3 presents  
 210 the obtained results, and Sec. 4 presents the conclusions.

## 211 **2 Experimental Setup**

212 The experimental device is the same as in Assis and Franklin (2020), consisting of  
 213 a water reservoir, two centrifugal pumps, a flow straightener, a 5-m-long closed-conduit  
 214 channel, a settling tank, and a return line, where a pressure-driven water flow was im-  
 215 posed in the order just described. The channel was made of transparent material and  
 216 had a rectangular cross section 160 mm wide and  $2\delta = 50$  mm high, its 1-m-long test  
 217 section starting 3 m downstream of the channel inlet. This corresponds to 40 hydraulic  
 218 diameters, which assured a developed channel flow upstream the bedforms. The remain-  
 219 ing 1-m-long section connected the exit of the test section to the settling tank. Figures  
 220 1d and 1a present, respectively, the layout of the experimental device and a photograph  
 221 of the test section.

222 Controlled grains were poured inside the channel, filled previously with water, form-  
 223 ing two conical piles that were afterward deformed into barchans by the imposed water  
 224 flow. The pairs of bedforms were formed in either aligned or off-centered configurations

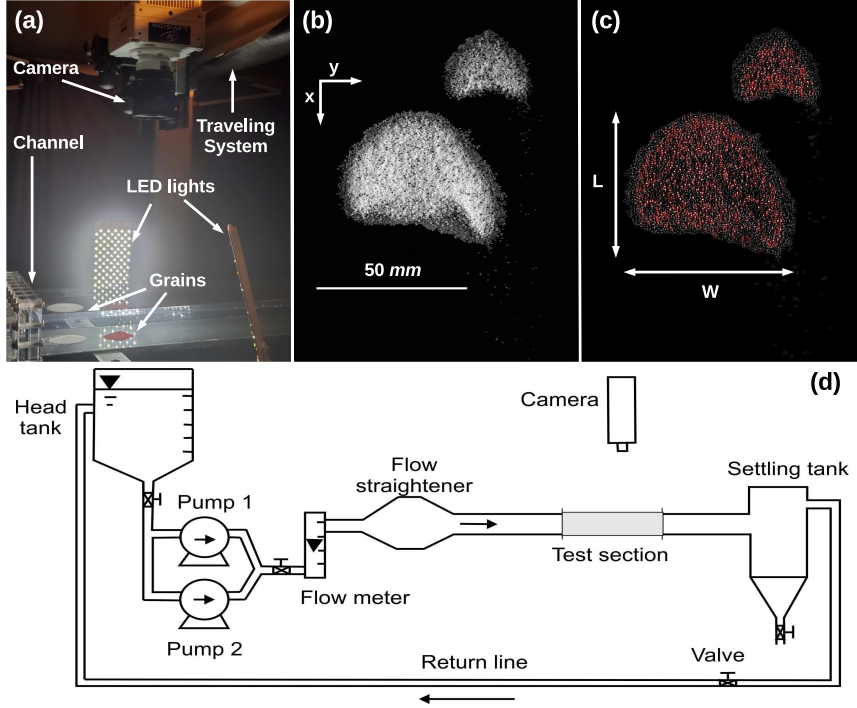


**Figure 1.** Experimental setup, barchans and grains detection, and definition of some geometrical parameters. (a) Photograph of the experimental setup showing the test section, camera, traveling system, LED lights, and dunes on the bottom wall of the channel. (b) Top-view image of two interacting barchans, the water flow is from top to bottom. (c) Binarized image of interacting barchans showing identified grains that were tracked along images and some of the barchan dimensions. (d) Layout of the experimental setup.

225 and the longitudinal distance between initial piles was of the order of the diameter of  
 226 the upstream pile. The size of the upstream dune (impact dune) was always equal or lesser  
 227 than that of the downstream dune (target dune), since the dune velocity varies inversely  
 228 with its size (Bagnold, 1941), their mass ratio varying within 0.021 and 1. We did not  
 229 impose an influx of grains coming from regions upstream the impact dune, so that the  
 230 entire system lost grains and decreased in mass along time. With that procedure, we ob-  
 231 tained binary interactions for all five patterns described in Assis and Franklin (2020),  
 232 in both aligned and off-centered configurations.

233 The ensemble of tests used tap water at temperatures within 25 and 28 °C and round  
 234 glass beads ( $\rho_s = 2500 \text{ kg/m}^3$ ) with diameters  $0.15 \text{ mm} \leq d_s \leq 0.25 \text{ mm}$  and  $0.40 \text{ mm}$   
 235  $\leq d_s \leq 0.60 \text{ mm}$  (not mixed with each other). In the following, we consider  $d$  as the  
 236 mean value of  $d_s$ . In order to facilitate the tracking of grains, tests focused on the mass  
 237 exchange between barchans used 96-98 % of white grains and 4-2 % of black grains, for  
 238 both dunes, and tests focused on particle diffusion at the grain scale used white grains  
 239 for the impact and red grains for the target dune (colors inverted with respect to Assis  
 240 and Franklin (2020)), all of them with the same density, diameter and roundness for a  
 241 given test. The cross-sectional mean velocity of water,  $U$ , was fixed at either 0.243 or  
 242 0.278 m/s (computed as the measured flow rate divided by the cross-sectional area), cor-  
 243 responding to Reynolds numbers based on the channel height,  $\text{Re} = \rho U 2\delta / \mu$ , of  $1.22 \times$   
 244  $10^4$  and  $1.39 \times 10^4$ , respectively, where  $\mu$  is the dynamic viscosity and  $\rho$  the density of  
 245 the fluid. The shear velocities on the channel walls in the absence of dunes,  $u_*$ , were com-

246 puted based on measurements with a two-dimensional two-component particle image ve-  
 247 locimetry (2D2C-PIV) device and found to follow the Blasius correlation (Schlichting,  
 248 2000), being 0.0141 and 0.0159 m/s for the two imposed water flows. By considering the  
 249 fluid velocities applied to each grain type, the Shields number,  $\theta = (\rho u_*^2)/((\rho_s - \rho)gd)$ ,  
 250 varied within 0.027 and 0.086, where  $g$  is the acceleration of gravity. Because the shear  
 251 velocity varies over the surface of each dune, as well as in some regions on the channel  
 252 walls when in the presence of barchans (Bristow et al., 2018, 2019, 2020), we use  $u_*$  (undis-  
 253 turbed by dunes) as the reference value for the fluid shearing. Microscopy images of the  
 254 used grains and a table summarizing the tested conditions are available in the support-  
 255 ing information.

256 The evolution of bedforms was recorded by either a high-speed or a conventional  
 257 camera mounted on a traveling system and placed above the channel, both the camera  
 258 and traveling system being controlled by a computer. The high-speed camera was of com-  
 259plementary metal-oxide-semiconductor (CMOS) type with maximum resolution of 2560  
 260px  $\times$  1600 px at 800 Hz, and we set its region of interest (ROI) within 2176 px  $\times$  960  
 261px and 2560 px  $\times$  1600 px and the frequency to 200 Hz. The field of view varied from  
 262117 mm  $\times$  75 mm to 205 mm  $\times$  112 mm, the area covered by each grain varying within  
 2636 to 32 px in the images. The conventional camera, also of CMOS type, had a max-  
 264imum resolution of 1920 px  $\times$  1080 px at 60 Hz, which were the ROI and frequency set  
 265in the tests. For the tests on the exchange pattern, the field of view was 160 mm  $\times$  90  
 266mm, the area covered by each grain ( $d = 0.2$  mm) corresponding thus to approximately  
 2675 px, while the tests on the merging pattern had a field of view of 260 mm  $\times$  146 mm,  
 268the area covered by each grain ( $d = 0.5$  mm) corresponding to approximately 11 px. We  
 269mounted lenses of 60 mm focal distance and F2.8 maximum aperture on the cameras and  
 270made use of lamps of light-emitting diode (LED) branched to a continuous-current source  
 271to provide the necessary light while preventing beating with the cameras. The conver-  
 272sion from px to a physical system of units was made by means of a scale placed in the  
 273channel previously filled with water. Movies showing the motion of grains over approach-  
 274ing and colliding barchans are available in the supporting information.

275 The acquired images were processed by numerical scripts written in the course of  
 276this work and based on Crocker and Grier (1996), Kelley and Ouellette (2011), Houssais  
 277et al. (2015) and Cúñez and Franklin (2020). They basically removed the image back-  
 278ground, binarized the images, identified the barchan morphology and individual grains,  
 279and computed the main morphological properties of bedforms, their relative distances  
 280and the motion of grains. Figures 1b and 1c present, respectively, raw and processed im-  
 281ages, the latter showing identified grains that were tracked along images.

282 Given its high frequencies, the high-speed camera uses an internal memory to store  
 283the acquired images, to be discharged to a computer once the measurements are over or  
 284the memory full. Depending on the tests, the time for discharging image files was greater  
 285than that for reaching the next stage of interaction between dunes. These were the cases  
 286of tests with higher velocities ( $U = 0.278$  m/s), for which once the images were discharged  
 287we had to restart the tests from the beginning, under the same conditions, until reach-  
 288ing the next stage to be recorded. For the other tests, measurements were made in a con-  
 289tinuous mode, the camera having discharged the files to the computer before the next  
 290stage was reached. We note that in spite of presenting the realization of one instance of  
 291each interaction stage, we recorded a large number of tests at normal (60 Hz) frequen-  
 292cies (123 of them presented in Assis and Franklin (2020)) and repeated the data acqui-  
 293sition of all tests at higher frequencies. We verified that the trajectories were consistent  
 294with the results presented here and, because of the large amount of data presented in  
 295this paper (for instance, 22 movies in the supporting information), we did not fully pro-  
 296cess all the data and do not show all of them here.

### 3 Results and discussion

Because in Assis and Franklin (2020) the ensemble of tests for each pattern showed the same behavior, we present next the motion of grains for one instance of each pattern, in both aligned and off-centered configurations.

#### 3.1 Trajectories of grains leaving dunes and mass exchange

We tracked moving grains during the interaction of barchans, and computed their trajectories. For these grains, the motion was mainly continuous, though with a stick-slip character, occurring directly over the channel wall (acrylic) and happening for a short time (that necessary for traveling from one barchan to the other). The trajectories of grains migrating from one dune to another, and also of grains leaving dunes and being entrained further downstream by the fluid, are of particular interest. Those trajectories reveal not only the masses exchanged between nearby dunes and lost by the entire system, but also details on how these exchanges and losses occur. Figures 2 to 6 show the trajectories of grains during different stages of barchan-barchan interactions, for all the five patterns in both aligned and off-centered configurations. Figures 2 to 6 correspond to the chasing, merging, exchange, fragmentation-chasing and fragmentation-exchange patterns (Assis & Franklin, 2020), respectively, where subfigures on the top are related to aligned and on the bottom to off-centered cases. Red lines correspond to grains leaving the upstream (impact) dune, blue lines to grains leaving the downstream (target) dune, white lines to grains migrating from a downstream bedform to the upstream one, and magenta lines to grains leaving a new bedform. Whenever the bedforms are not the original impact and target barchans (case of white trajectories), the upstream bedform is considered as the one whose centroid is in an upstream position with respect to the other bedform. For the sake of clarity, the trajectories of a small portion of grains are plotted in Figures 2 to 6 (in average, 45% of trajectories that took place during approximately 9 s were plotted, but percentages vary from 5% to 100% depending on the case), all trajectory types being shown, however.

For the chasing pattern (Figure 2), the wake of the upstream barchan strongly affects the downstream one (Bristow et al., 2018, 2019, 2020), the downstream barchan being strongly eroded and, due to small asymmetries, becoming eventually off-centered even in the aligned case. We observe a large number of grains leaving the downstream barchan (in the aligned case, once dunes become off-centered), and the asymmetry of horns increases due to grains received asymmetrically from the upstream barchan. With both cases being eventually in an off-centered configuration, only grains from one of the horns of the upstream barchan reach the downstream one, and part of them simply go around the downstream barchan. At that stage (Figures 2b and 2d), we measured that approximately 25% of grains leaving the upstream barchan go over the downstream dune (24% in the aligned and 28% in the off-centered case, which correspond to mass flow rates of  $4.60 \times 10^{-3}$  and  $1.12 \times 10^{-3}$  g/s, respectively), and that 7% go around it and 69% are directly entrained further downstream in the aligned case (mass flow rates of  $1.34 \times 10^{-3}$  and  $1.32 \times 10^{-2}$  g/s, respectively), while 44% go around the downstream barchan and 28% are directly entrained further downstream in the off-centered case (mass flow rates of  $1.75 \times 10^{-3}$  and  $1.12 \times 10^{-3}$  g/s, respectively). In addition, we computed the difference between grains received and lost by the downstream barchan (still at the late stage) and found that it reaches deficits of 18% and 33% in the aligned and off-centered cases, respectively (net flow rates of  $3.45 \times 10^{-3}$  and  $1.32 \times 10^{-3}$  g/s, respectively). The measured deficits corroborate the size decrease of the downstream barchan in the chasing pattern.

For the merging pattern (Figure 3), we observe some differences between the aligned and off-centered cases. At the initial stage of the aligned case, a great part of grains leav-

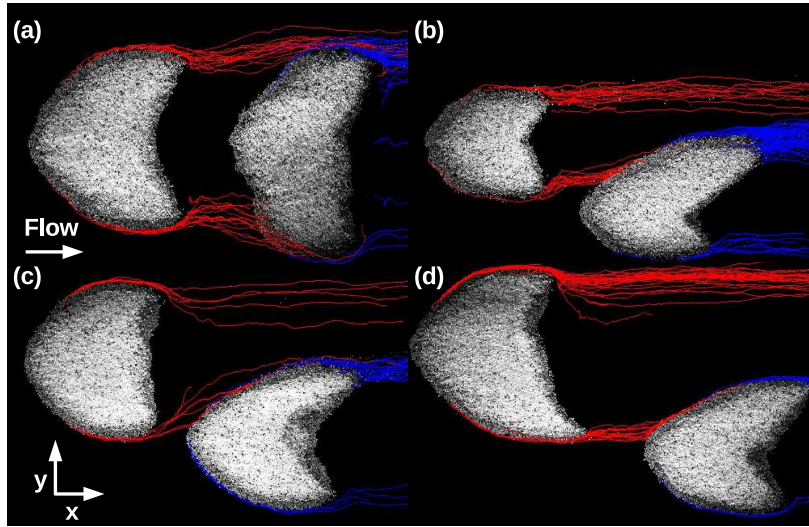


**Figure 2.** Trajectories of some grains at two different intervals for the chasing pattern. Figures (a) and (b) correspond to two different stages of the interaction for the aligned case, and figures (c) and (d) to two different stages for the off-centered case. Red lines correspond to grains leaving the upstream dune and blue lines to grains leaving the downstream one.

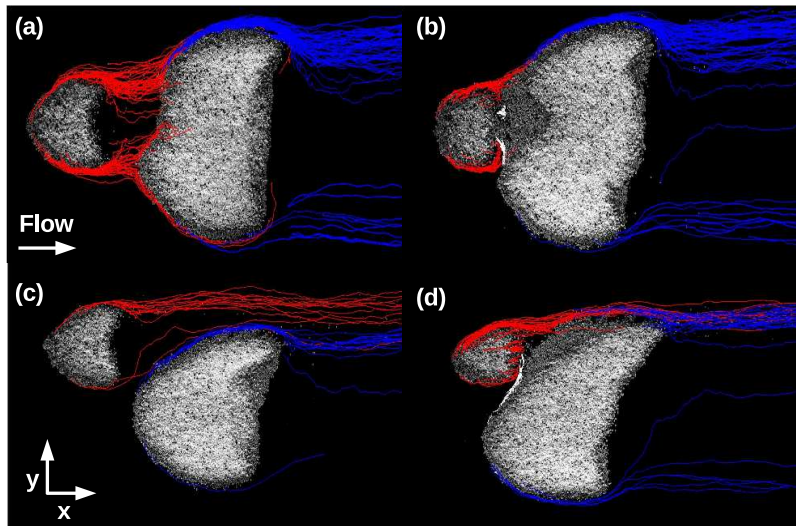


**Figure 3.** Trajectories of some grains at two different intervals for the merging pattern. Figures (a) and (b) correspond to two different stages of the interaction for the aligned case, and figures (c) and (d) to two different stages for the off-centered case. Red lines correspond to grains leaving the upstream dune, blue lines to grains leaving the downstream one, and white lines to grains migrating from the downstream bedform to the upstream one.

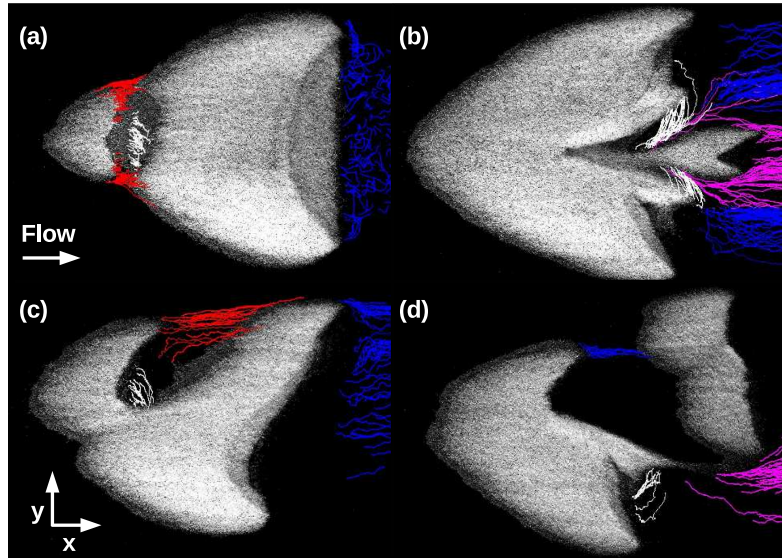


**Figure 4.** Trajectories of some grains at two different intervals for the exchange pattern. Figures (a) and (b) correspond to two different stages of the interaction for the aligned case, and figures (c) and (d) to two different stages for the off-centered case. Red lines correspond to grains leaving the upstream dune, blue lines to grains leaving the downstream one, white lines to grains migrating from the downstream bedform to the upstream one, and magenta lines to grains leaving the new bedform.

348 ing the upstream dune reaches the downstream one (92% of grains are incorporated by  
 349 the downstream bedform, which corresponds to  $3.69 \times 10^{-3}$  g/s), deforming the down-  
 350 stream barchan into a barchanoid form. At a later stage, when dunes are almost collid-  
 351 ing, the recirculation region in the wake of the upstream barchan carries grains from the  
 352 downstream bedform to the upstream one, eroding the toe of the downstream bedform  
 353 and forming a monolayer carpet between dunes before merging occurs. In the off-centered  
 354 case, the main differences are that a much smaller number of grains leaving the upstream  
 355 dune at the initial stage reaches the downstream one (only 1% of them, correspond-  
 356 ing to  $3.65 \times 10^{-5}$  g/s), and that, before merging occurs, the recirculation region of the up-  
 357 stream barchan does not strongly erode the leading edge of the downstream dune, form-  
 358 ing only the monolayer carpet.

359 During the initial stages, the behaviors of the exchange pattern in aligned and off-  
 360 centered configurations (Figures 4a and 4c) are similar to those of the merging pattern  
 361 (Figures 3a and 3c), the main difference being that grains leave the target barchan along  
 362 all the lee face, instead of only through the horns. In the off-centered case, grains do not  
 363 leave the target barchan from its horn farther from the upstream dune. This transverse  
 364 distribution of the granular flux is caused by disturbances in the fluid flow (due to the  
 365 upstream barchan), the flux of parting grains being concentrated out of horns in the case  
 366 of an isolated barchan, as shown in the supporting information. We note that in Figure  
 367 4a the field of view does not allow us to follow the parting grains further downstream.  
 368 However, during the tests we noticed that, indeed, a part of grains is entrained further  
 369 downstream from the avalanche/lee face. After collision has taken place, the perturba-  
 370 tion caused by the impacting barchan leads the resulting bedform to eject a new barchan.  
 371 Along this text, we refer sometimes to the resulting (merged) and ejected bedforms as  
 372 *parent* and *baby* barchans, respectively. In the aligned case, the new barchan is ejected

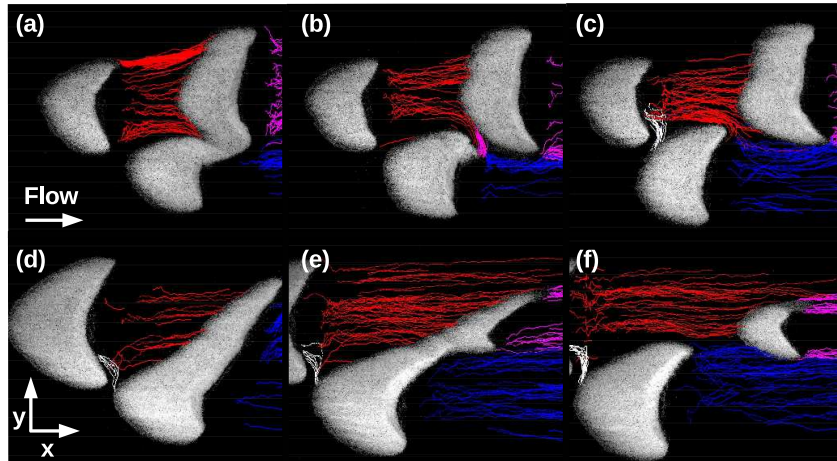


**Figure 5.** Trajectories of some grains at three different intervals for the fragmentation-chasing pattern. Figures (a), (b) and (c) correspond to three different stages of the interaction for the aligned case, and figures (d), (e) and (f) to three different stages for the off-centered case. Red lines correspond to grains leaving the upstream dune, blue lines to grains leaving the downstream one, white lines to grains migrating from the downstream bedform to the upstream one, and magenta lines to grains leaving a new bedform.

373 from a central position at the lee face, and we observe that a considerable part of grains  
 374 migrate from the new ejected barchan toward the upstream bedform (22% of the grains  
 375 that leave the new barchan, corresponding to  $1.02 \times 10^{-3}$  g/s), forming two branches  
 376 connecting, during a certain period, both dunes. In the off-centered case, the new barchan  
 377 is ejected from one of the horns, and grains do not migrate from the ejected barchan to-  
 378 ward the upstream dune. Instead, the ejected barchan continues receiving grains from  
 379 the upstream dune.

380 In the fragmentation-chasing pattern (Figure 5), the perturbation caused by the  
 381 wake of the upstream barchan is so strong that it splits the downstream dune into two  
 382 smaller barchans. In both the aligned and off-centered cases, the downstream dune re-  
 383 ceives grains from the upstream barchan, but loses a larger quantity of grains (reaching  
 384 deficits of 73% and 19% in the aligned and off-centered cases, respectively, which cor-  
 385 respond to  $3.92 \times 10^{-4}$  and  $7.92 \times 10^{-5}$  g/s). Because of the perturbation of the fluid  
 386 flow, grains leave barchans along the lee face, the exception being the smaller of split barchans  
 387 of the off-centered case (perhaps also in the aligned case, but we did not follow it far-  
 388 ther in the channel given the limitations of our traveling system). Once divided, the new  
 389 barchans travel faster than the upstream one and they do not collide. However, one of  
 390 the new barchans remains for some time close to the upstream one and some of its grains  
 391 migrate toward the latter, entrained by the recirculation region.

392 The fragmentation-exchange pattern (Figure 6) is roughly similar to the fragmentation-  
 393 chasing one, the main difference being that the impact barchan collides with one of the  
 394 split bedforms. During the collision process, some grains are entrained from the down-  
 395 stream dune toward the impact barchan by the wake of the latter. In the aligned case,  
 396 grains entrained further downstream leave barchans through one of the horns (mainly

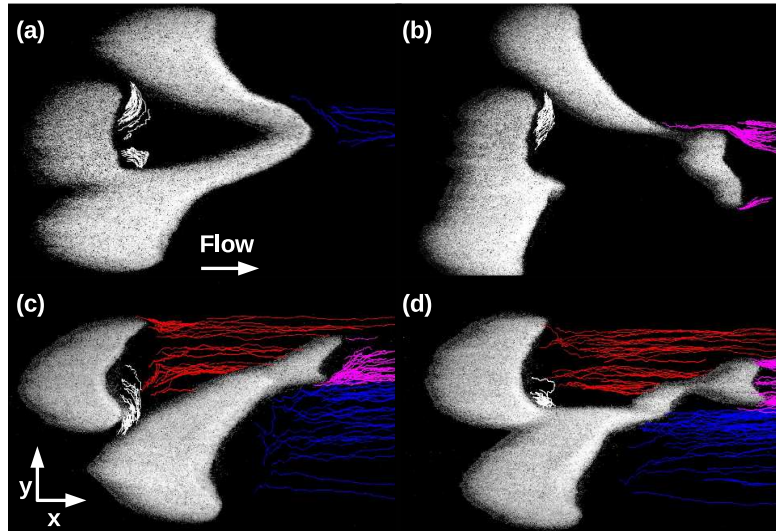


**Figure 6.** Trajectories of some grains at two different intervals for the fragmentation-exchange pattern. Figures (a) and (b) correspond to two different stages of the interaction for the aligned case, and figures (c) and (d) to two different stages for the off-centered case. Red lines correspond to grains leaving the upstream dune, blue lines to grains leaving the downstream one, white lines to grains migrating from the downstream bedform to the upstream one, and magenta lines to grains leaving a new bedform.

397 through the shared horn), while in the off-centered case parting grains are distributed  
 398 along the lee face. Around 45% of the grains leaving the downstream bedforms migrate  
 399 to the impact barchan in the aligned case (46% and 42% in Figures 6a and 6b, respec-  
 400 tively, which correspond to  $6.55 \times 10^{-5}$  and  $4.31 \times 10^{-5}$  g/s), while the percentages are  
 401 70% and 5% for the two stages of the off-centered case shown in Figures 6c and 6d, re-  
 402 spectively (corresponding to  $1.69 \times 10^{-3}$  and  $8.05 \times 10^{-5}$  g/s). In the aligned case these  
 403 percentages consider both split bedforms, while those for the off-centered case consider  
 404 only grains from the split bedform closer to the impact barchan. The high percentage  
 405 found in the approaching of barchans in the off-centered case (Figure 6c) reflects the for-  
 406 mation of a granular bridge between them, which, once formed, unite both barchans with  
 407 the consequent decrease in grains entrained toward the upstream dune (Figure 6d).

408 The chasing and fragmentation-chasing patterns are, perhaps, the three-dimensional  
 409 equivalent of the dune-dune repulsion identified by Bacik et al. (2020) in a narrow Couette-  
 410 type circular channel, where the wake of the upstream bedform intensifies erosion on the  
 411 downstream one, increasing the celerity of the latter. However, different from Bacik et  
 412 al. (2020), our channel is relatively large, producing dune-dune repulsion cases where barchans  
 413 become off-centered and split (in addition to the collision cases).

414 A table summarizing the percentages of grains exchanged between dunes, the to-  
 415 tal number of moving grains and the considered time interval is available in the support-  
 416 ing information. With that, we can estimate the overall transport of grains in the inter-  
 417 dune space (migrating from one dune to another or being entrained further downstream),  
 418 which is also presented in the supporting information (in terms of mass flow rates). In  
 419 addition, trajectories of grains leaving an isolated subaqueous barchan are also available  
 420 in the supporting information, from which we can observe that all grains leave the dune

421 through their horns (a great part of them coming from upstream regions and going around  
 422 the dune before reaching the horns, as shown by Alvarez and Franklin (2018) and Alvarez  
 423 and Franklin (2019)).

### 424 3.2 Lengths and velocities of exchanged grains

425 Based on grain trajectories, we identified, for the characteristic routes distinguished  
 426 in Subsection 3.1, typical lengths and velocities of grains migrating from one dune to an-  
 427 other. For that, we computed the displacement lengths in the longitudinal and trans-  
 428 verse directions,  $\Delta x$  and  $\Delta y$ , respectively, as well as the time-averaged velocities in the  
 429 longitudinal and transverse directions,  $V_x$  and  $V_y$ , respectively, of exchanged particles.  
 430 Displacements were computed as the differences between the final and initial positions  
 431 of each grain from their departure from one dune until reaching another one, and aver-  
 432 age velocities as the mean values for each grain during its migration. We then plotted  
 433 their respective probability distributions (PDs) by considering all tracked particles, and  
 434 present some of them in Figures 7 and 8 (other PDs are available in the supporting in-  
 435 formation, including those for an isolated barchan). While the velocities were normal-  
 436 ized by  $u_*$ , which is a characteristic velocity at the grain scale, lengths were normal-  
 437 ized by  $L_{drag} = \rho_s \rho^{-1} d$  (Hersen et al., 2002). Although the saturation length  $L_s$  proposed  
 438 by Pähtz et al. (2013) is the proper scale for the response of a granular bed to flow changes,  
 439 and, therefore, for erosion and deposition and minimum bedform scales, we use  $L_{drag}$   
 440 for normalizations.  $L_s$  takes into account the forces controlling grain and fluid relaxation,  
 441 both for gases and liquids, incorporating mechanisms not present in  $L_{drag}$ . However,  $L_{drag}$   
 442 is a length scale of inertial nature with a simple expression proposed by Hersen et al. (2002),  
 443 being a reasonable scaling for dune lengths over 5 orders of magnitude (Claudin & An-  
 444 dreotti, 2006).

445 Figure 7 presents PDs of grains migrating from upstream to downstream barchans,  
 446 and Figure 8 of those migrating from downstream to upstream bedforms. Distances and  
 447 velocities for the remaining cases are similar to those shown in Figures 7 and 8, and some  
 448 of them are presented in the supporting information, as well as those for a single barchan.  
 449 In general, mean values of traveled distances in the longitudinal direction are propor-  
 450 tional to the longitudinal separation between barchans, while in the transverse direction  
 451 they are proportional to the transverse offset between bedforms. Because exchanged grains  
 452 move directly over the channel wall (acrylic) when traveling from one barchan to another,  
 453 defining an area over which they move is more difficult than for grains moving over a thick  
 454 granular bed. However, distributions of  $\Delta x$  and  $\Delta y$  can be used to estimate the area swept  
 455 by the tracked grains: for grains moving in the longitudinal direction, that area is pro-  
 456 portional to  $\Delta x$  multiplied by 2 times the standard deviation of  $\Delta y$ , and the contrary  
 457 (in terms of  $x$  and  $y$ ) for grains moving in the transverse direction. Since we performed  
 458 Lagrangian tracking, another area of interest is the cross-sectional area crossed by the  
 459 followed particles. Because the exchanged grains roll directly over the channel wall, the  
 460 height of that area is proportional to the grain diameter, while its width is proportional  
 461 to the standard deviations of  $\Delta y$  or  $\Delta x$  for grains moving in the longitudinal or trans-  
 462 verse directions, respectively. Therefore, bedload fluxes can be estimated as the mass flow  
 463 rates divided by the corresponding cross-sectional areas. Concerning specifically the val-  
 464 ues of  $\Delta y/L_{drag}$  measured for barchan-barchan interactions, they have mean values and  
 465 standard deviations higher than those for the single dune (that has mean average and  
 466 standard deviation of -0.62 and 3.16, respectively). In particular, for cases where chan-  
 467 neling is present (red trajectories in Figures 2b, 3c, 3d and 5c, for example),  $\Delta y/L_{drag}$   
 468 reaches values one or two orders of magnitude higher than those for the single dune, in-  
 469 dicated a strong deflection in the trajectories of grains (values available in the support-  
 470 ing information).

471 For the longitudinal component of velocities, mean values are mostly positive but  
 472 can be negative when grains are entrained by the recirculation region of the upstream

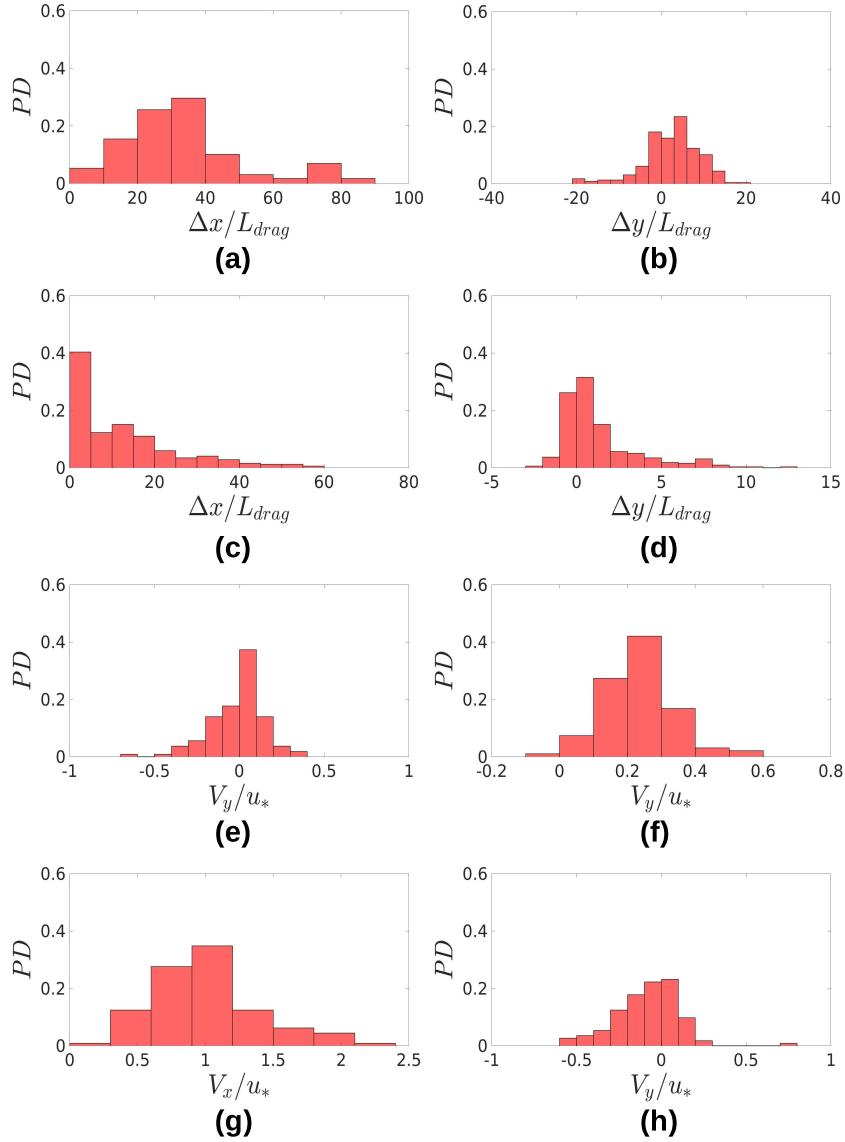


**Figure 7.** PDFs of total distances traveled by grains in longitudinal and transverse directions,  $\Delta x$  and  $\Delta y$ , respectively, normalized by  $L_{drag}$ , and PDFs of time-averaged velocities in the longitudinal and transverse directions,  $V_x$  and  $V_y$ , respectively, normalized by  $u_*$  (values of  $u_*$  are available in the supporting information). Figures (a) and (b) correspond to red trajectories in Figure 3a, with mean values of  $\Delta x/L_{drag} = 33.4$  and  $\Delta y/L_{drag} = 2.4$ , and standard deviations of, respectively,  $18.2$  and  $6.7L_{drag}$ . Figures (c) and (d) correspond to red trajectories in Figure 3d, with mean values of  $\Delta x/L_{drag} = 12.6$  and  $\Delta y/L_{drag} = 1.3$ , and standard deviations of, respectively,  $12.7$  and  $2.4$ . Figures (e) and (f) correspond to red trajectories in Figures 2a and 2b with mean values of  $V_y/u_*$  equal to  $-0.01$  and  $0.23$ , and standard deviations of  $0.16$  and  $0.10$ , respectively. Figures (g) and (h) correspond to red trajectories in Figure 5c (grains leaving the impact barchan along its lee face), with mean values of  $V_x/u_* = 1.01$  and  $V_y/u_* = -0.08$ , and standard deviations of  $0.39$  and  $0.19$ , respectively.

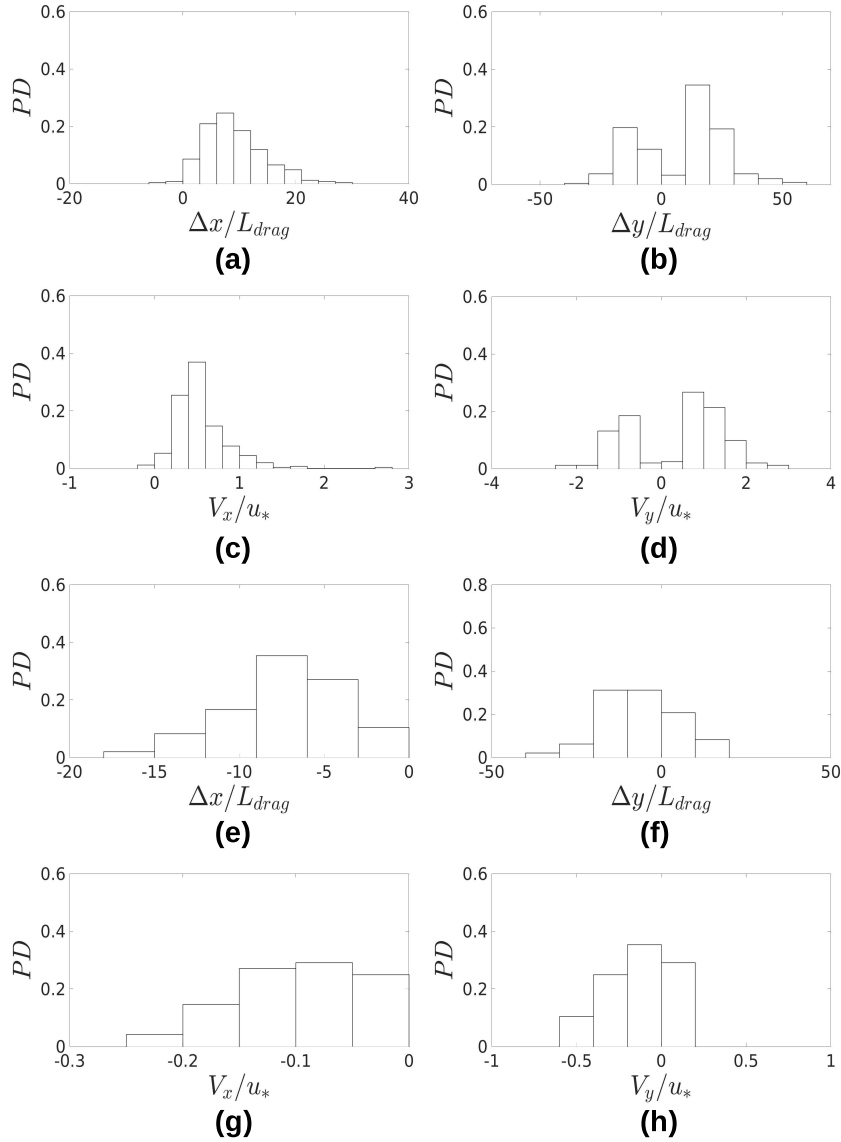


**Figure 8.** PDs of total distances traveled by grains in longitudinal and transverse directions,  $\Delta x$  and  $\Delta y$ , respectively, normalized by  $L_{drag}$ , and PDs of time-averaged velocities in the longitudinal and transverse directions,  $V_x$  and  $V_y$ , respectively, normalized by  $u_*$  (values of  $u_*$  are available in the supporting information). Figures (a) to (d) correspond to white trajectories in Figure 4b, with mean values for lengths of  $\Delta x/L_{drag} = 9.1$  and  $\Delta y/L_{drag} = 8.0$  and standard deviations of, respectively, 5.4 and 17.8, and mean values for velocities of  $V_x/u_* = 0.55$  and  $V_y/u_* = 0.37$ , and standard deviations of 0.31 and 1.13, respectively. Figures (e) to (h) correspond to white trajectories in Figure 6a, with mean values for lengths of  $\Delta x/L_{drag} = -7.2$  and  $\Delta y/L_{drag} = -6.3$  and standard deviations of, respectively, 3.5 and 11.4, and mean values for velocities of  $V_x/u_* = -0.10$  and  $V_y/u_* = -0.14$ , and standard deviations of 0.06 and 0.18, respectively.

473 dune, which happens in some cases when two bedforms are very close, almost touching  
 474 each other. In the main, they are one order of magnitude smaller than the undisturbed  
 475 shear velocity over the channel wall (reference value),  $u_*$ , but in some regions where the  
 476 fluid flow is locally accelerated and/or has its turbulence level increased  $V_x$  reaches val-  
 477 ues of the same order of magnitude of  $u_*$  (same order of magnitude found for grains leav-  
 478 ing an isolated barchan, shown in the supporting information). For the transverse com-  
 479 ponent, mean values tend to zero for aligned bedforms, due to symmetry, and deviate  
 480 from zero for off-centered bedforms (for reference, values for grains leaving an isolated  
 481 barchan have an average of the order of  $10^{-3}u_*$ ). For some aligned bedforms, such as dur-  
 482 ing the ejection of a baby barchan in the aligned-exchange configuration, distributions  
 483 of transverse displacements and velocities are bimodal and roughly symmetrical around  
 484 a zero mean. In particular, we found that the grains migrating from the baby barchan  
 485 toward the parent dune in the aligned-exchange configuration move downstream, with  
 486 mean longitudinal distances of approximately  $10L_{drag}$  and transverse displacements of  
 487 approximately  $15L_{drag}$ . For the chasing pattern in aligned configuration, mean values  
 488 of  $V_y/u_*$  deviate from approximately zero toward other values (from -0.01 to 0.23 in the  
 489 case of Figures 7e and 7f), this being a consequence of wake interactions, including chan-  
 490 neling, that lead the aligned configuration toward an off-centered one. In all interact-  
 491 ing cases, wake effects and small asymmetries are present, the mean value of  $V_y/u_*$  for  
 492 the single dune being at least one order of magnitude smaller when compared to all cases  
 493 ( $V_y/u_* = -0.006$  for the single dune).

### 494 3.3 Spreading after collision

495 Having analyzed in Subsections 3.1 and 3.2 the motion of grains between bedforms,  
 496 we investigate now the motion, after collision has taken place, of grains originally in the  
 497 impact barchan. For that, we present data at both the barchan and grain scales. At the  
 498 barchan scale, some of the images obtained by Assis and Franklin (2020) are now fur-  
 499 ther treated for measuring the spreading of the impacting bedform based on the evolu-  
 500 tion of its area over the target barchan. At the grain scale, we determine, from new movies,  
 501 typical trajectories of individual grains by tracking their motion once collision has oc-  
 502 curred.

503 We notice two distinct stages in the evolution of the impacting bedform in the merg-  
 504 ing and exchange cases. The first stage corresponds to a barchan shape being stretched  
 505 and becoming a longitudinal stripe, while in the second one the stripe widens slowly along  
 506 time. Both stages can be observed in Figures 9 to 11, which show grains from the im-  
 507 pact barchan over the target one, and also in the supporting information, which shows  
 508 the width of the longitudinal stripe  $W_d$  as a function of time. We note that a two-stage  
 509 adaptation of dunes to a change in the flow conditions has already been proposed by Fischer  
 510 et al. (2008). Based on 2D simulations using a minimum model (Kroy et al., 2002a, 2002b),  
 511 they showed that dunes are unstable solutions: once disturbed, a first stage that corre-  
 512 sponds to an adaptation of shape to the new unstable conditions takes place, followed  
 513 by a second stage where mass changes along these new conditions. This seems to bear  
 514 similarities with the spreading of the impact barchan after collision takes place. How-  
 515 ever, while the initial flattening can in part be explained as an adaptation to new con-  
 516 ditions, sharing perhaps similarities with Fischer et al. (2008), the transverse diffusion  
 517 does not seem related to numerical results based on 2D bedforms since the widening of  
 518 the longitudinal stripe results from a diffusion-like mechanism over the resulting barchan,  
 519 not acting directly on the same bedform (the impact barchan, which has flattened in the  
 520 first stage).

521 For the first stage, Figures 9 and 10 show how grains originally in the impact barchan  
 522 spread over the target one during merging and exchange processes, respectively, in the  
 523 aligned case. Red (clear) regions correspond to grains from the impact barchan and white  
 524 (darker) to grains from the target one, and different instants are shown from top to bot-

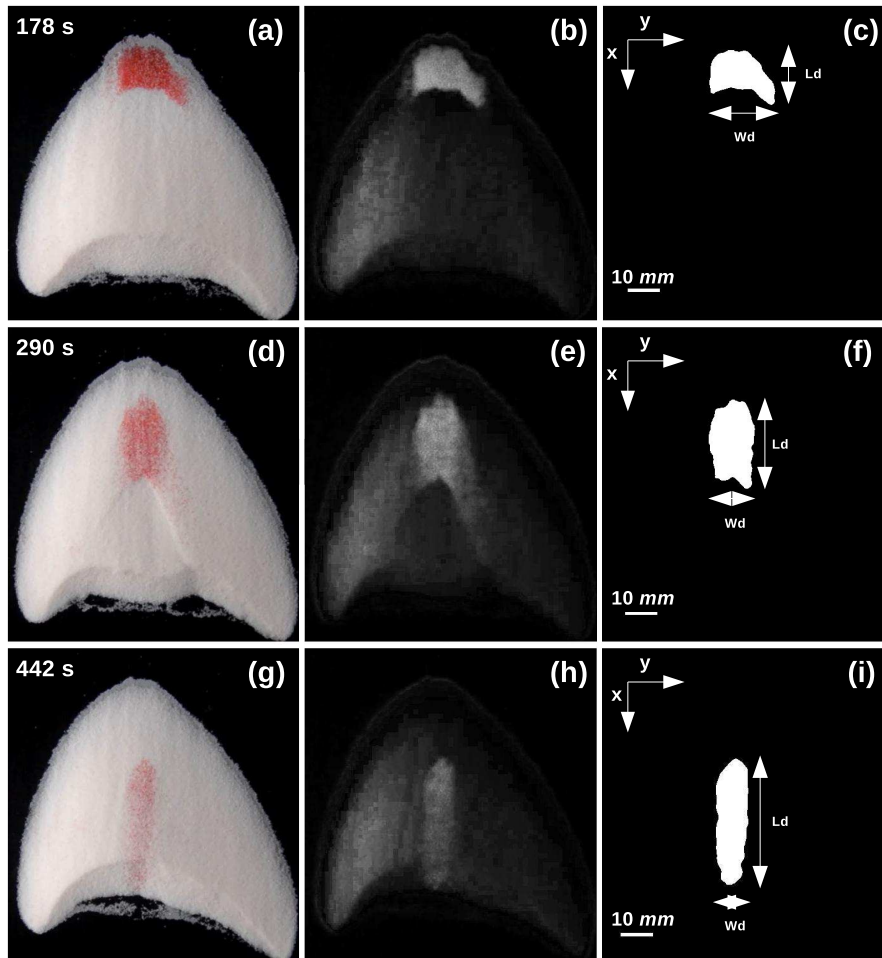


**Figure 9.** Distribution of grains from the impact barchan over the target one during a merging process in the aligned case. Red (clear in figures b, e and h) grains come from the impact barchan and white (darker in figures b, e and h) grains are from the target one. From top to bottom, figures correspond to different instants (shown in figures), and from left to right figures correspond to raw, grayscale and binary images.  $L_d$  is the length and  $W_d$  the width of the structure formed with grains from the impact barchan.

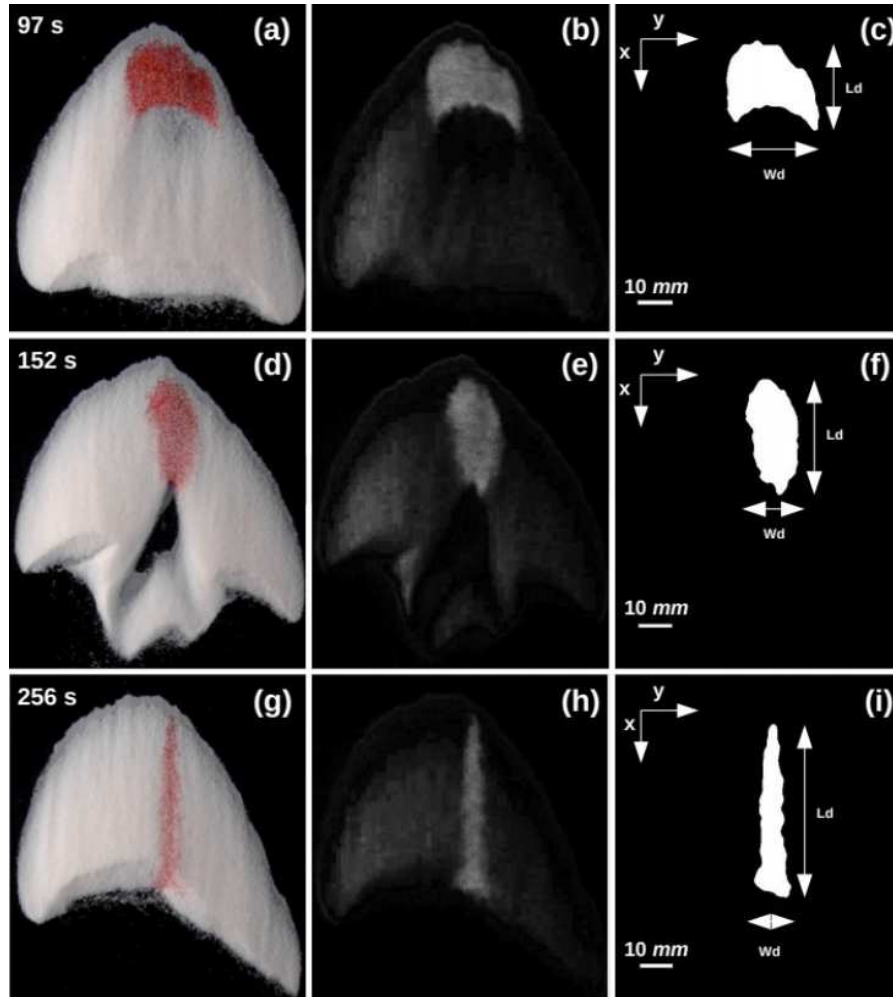


**Figure 10.** Distribution of grains from the impact barchan over the target one during an exchange process in the aligned case. Red (clear in figures b, e and h) grains come from the impact barchan and white (darker in figures b, e and h) grains are from the target one. From top to bottom, figures correspond to different instants (shown in figures), and from left to right figures correspond to raw, grayscale and binary images.  $L_d$  is the length and  $W_d$  the width of the structure formed with grains from the impact barchan.

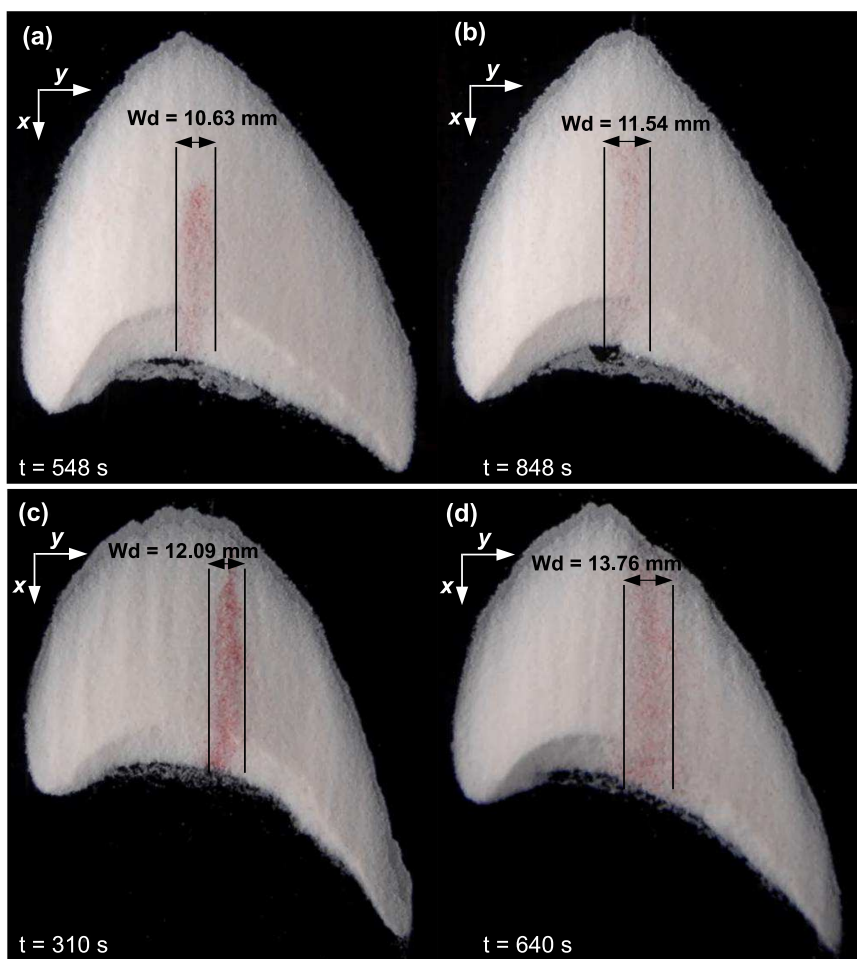


**Figure 11.** Second stage of the spreading of grains from the impact dune over the target one during (a) and (b) merging and (c) and (d) exchange processes. Red grains come from the impact barchan. Times and lengths are shown in the figure.

525 tom. We observe that, while the impacting bedform is deformed into a longitudinal stripe,  
 526 its wake disturbs the surface of the target barchan. In the case of the exchange pattern,  
 527 the perturbation is strong enough to eject a new barchan that does not contain grains  
 528 from the impact dune, while in the merging pattern the perturbation is attenuated. The  
 529 difference in patterns may be related to the lengths of surface waves, that propagate faster  
 530 than the resulting barchan and, if not attenuated, can eject a new barchan by calving  
 531 (Elbelrhiti et al., 2005; Worman et al., 2013). Claudin and Andreotti (2006) showed that  
 532 the minimum wavelength for subaqueous waves is approximately 20 mm, meaning that  
 533 only waves longer than that value persist and produce calving. If we consider the initial  
 534 values of  $W_d$  as the typical length of the impact barchan, then  $W_d < 20$  mm for the  
 535 merging and  $W_d > 20$  mm for the exchanges patterns, in accordance with Claudin and  
 536 Andreotti (2006) (see the supporting information for the evolutions of  $W_d$  along time).  
 537 The ejection of a baby barchan seems thus in accordance with the calving mechanism,  
 538 as proposed by Elbelrhiti et al. (2005) and Worman et al. (2013).

539 Figure 11 presents the second stage of the deformation of the impacting bedform,  
 540 Figures 11a and 11b corresponding to a merging process and Figures 11c and 11d to an  
 541 exchange process. We observe that the longitudinal stripe widens slowly along time, in

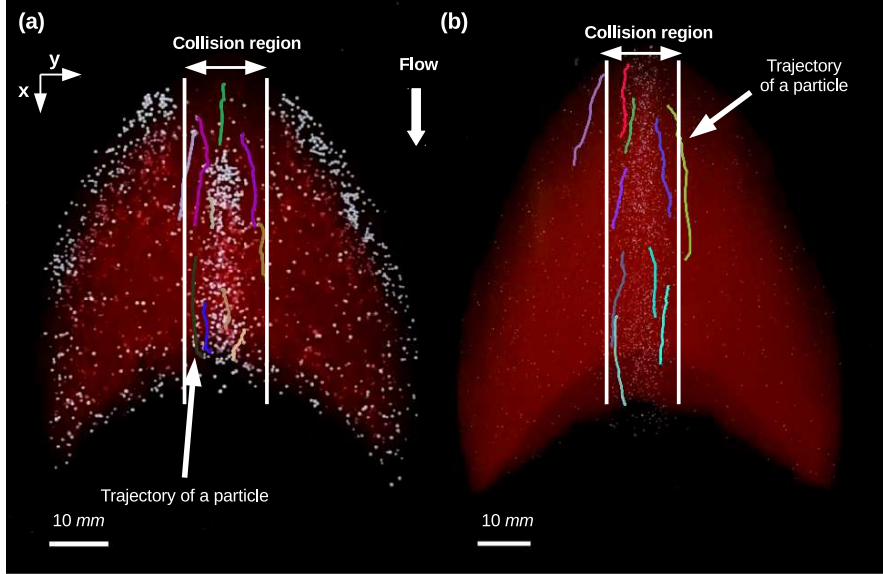


**Figure 12.** Typical trajectories of individual grains from the impact barchan over the target one for (a) merging and (b) exchange.

542 what resembles a diffusion process, taking 300 s to widen 0.91 mm in the merging case  
 543 and 330 s to widen 1.67 mm in the exchange case. The corresponding expansion (widen-  
 544 ing) velocities are, respectively,  $3 \times 10^{-6}$  and  $5 \times 10^{-6}$  m/s, which correspond to  $2 \times$   
 545  $10^{-4}$  and  $3 \times 10^{-4} u_*$ , while grain velocities are much larger, of the order of  $10^{-1} u_*$  (as  
 546 as shown next). Because the main flow is in the longitudinal direction, we conjecture that  
 547 the widening of the longitudinal stripe is caused by the erratic trajectories of grains, which  
 548 are, in addition, amplified in the transverse direction due to the lateral slopes of the bed-  
 549 form. Although not a pure diffusion in the strict sense, we describe next this widening  
 550 processes as a diffusion-like mechanism given the resemblance. In order to investigate  
 551 that, we followed individual grains during the stripe widening and computed their tra-  
 552 jectories, displacement lengths and velocities.

553 Figures 12a and 12b show some trajectories of grains (from the impact dune) over  
 554 the target barchan for the merging and exchange processes, respectively. The motion of  
 555 these grains was intermittent and occurred from a starting point until reaching the crest  
 556 region. We observe a small transverse component that varies from grain to grain that  
 557 contributes to the stripe widening. In order to scrutinize their relation, we computed mean  
 558 values and standard deviations of displacements and velocities for a large amount of par-  
 559 ticles, obtaining diffusion-like measurements at the grain scale. The considered grains  
 560 were those from the impact barchan that started moving over the target barchan at po-  
 561 sitions within a width equivalent to that of the impact dune (boundaries shown in Fig-  
 562 ure 12).

563 Figure 13 presents PDs of total distances traveled by the followed grains in the lon-  
 564 gitudinal and transverse directions,  $\Delta x$  (Figures 13a and 13c) and  $\Delta y$  (Figures 13b and  
 565 13d), respectively. These distances correspond to the differences between the final and  
 566 initial positions of each grain, and they are normalized by  $L_{drag}$ . Figures 13a and 13b  
 567 correspond to the merging and Figures 13c and 13d to the exchange pattern. PDs of  $\Delta x/L_{drag}$   
 568 have a decreasing distribution that seems exponential, but we prefer to not assert its form

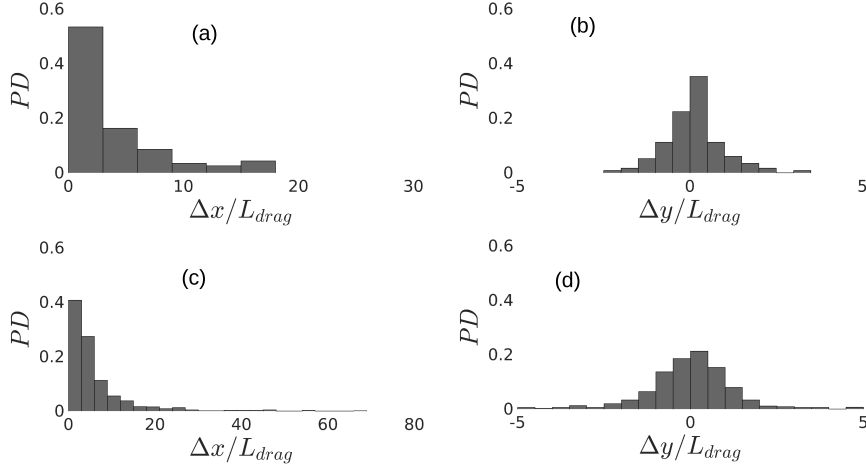


**Figure 13.** PDs of total distances traveled by grains in: (a) and (c) the longitudinal direction and (b) and (d) the transverse direction,  $\Delta x$  and  $\Delta y$ , respectively, normalized by  $L_{drag}$ . Figures (a) and (b) correspond to the merging and (c) and (d) to the exchange pattern.

569 for the moment, however, given the relative small size of our samples. Longitudinal dis-  
 570 tances have average values of approximately 4 and  $6L_{drag}$  and RMS (root mean square)  
 571 averages of 5 and  $10L_{drag}$  for the merging and exchange patterns, respectively. Distri-  
 572 butions of  $\Delta y/L_{drag}$  show a Gaussian-like behavior, peaked close to zero. Here again,  
 573 we prefer to not assert the form of the distribution. Transverse distances traveled by the  
 574 followed grains show average values of approximately 0.1 and  $-0.2L_{drag}$ , standard devi-  
 575 ations of 0.8 and  $1.5L_{drag}$ , and RMS averages of 0.8 and  $1.5L_{drag}$  for the merging and  
 576 exchange patterns, respectively. These values show ensemble averages around zero with  
 577 large dispersions, indicating that grains travel longitudinally with considerable devi-  
 578 ations in the transverse direction that are symmetrical with respect to the longitudinal  
 579 direction. This kind of trajectory spreads the longitudinal stripe in a way that resem-  
 580 bles a diffusion mechanism.

581 Figure 14 presents mean velocities of grains during their trajectories in the longi-  
 582 tudinal and transverse directions,  $V_x$  (Figures 14a and 14c) and  $V_y$  (Figures 14b and 14d),  
 583 respectively, normalized by  $u_*$ . Each mean value in the PDs was computed as the time-  
 584 averaged velocity of each grain during its displacement over the dune. PDs of  $V_x$  show  
 585 a decreasing distribution that is monotonic for the merging and non-monotonic for the  
 586 exchange pattern. The mean velocities in the longitudinal direction are of the order of  
 587  $0.1u_*$ :  $V_x$  presents average values of 0.07 and  $0.08u_*$ , standard deviations of 0.06 and  $0.08u_*$ ,  
 588 and RMS averages of 0.09 and  $0.11u_*$  for the merging and exchange patterns, respec-  
 589 tively. PDs of  $V_y$  are peaked close to zero, and present average values of approximately  
 590  $4.0 \times 10^{-4}$  and  $-1.5 \times 10^{-3}u_*$ , standard deviations of approximately  $1.0 \times 10^{-2}$  and  $1.4$   
 591  $\times 10^{-2}u_*$ , and RMS averages of  $9.5 \times 10^{-3}$  and  $1.4 \times 10^{-2}u_*$  for the merging and ex-  
 592 change patterns, respectively. As for  $\Delta y$ , transverse velocities present an ensemble av-  
 593 erage around zero with large dispersion, indicating motions in the transverse direction  
 594 that are symmetrical with respect to the longitudinal direction. For each grain, we com-  
 595 puted the RMS average of the transverse velocity,  $V_{y_{rms}}$ , during its trajectory over the  
 596 barchan, and present the corresponding PDs in supporting information. From the RMS  
 597 PDs, we find average values of  $3 \times 10^{-4}$  and  $7 \times 10^{-4}u_*$  ( $5 \times 10^{-6}$  and  $11 \times 10^{-6}$  m/s)  
 598 for the merging and exchange cases, respectively. These values are of the same order of  
 599 magnitude of those obtained for the expansion of the longitudinal stripe. PDs of  $\Delta x$ ,  $\Delta y$ ,  
 600  $V_x$ ,  $V_y$  and  $V_{y_{rms}}$  in dimensional form are available in the supporting information.

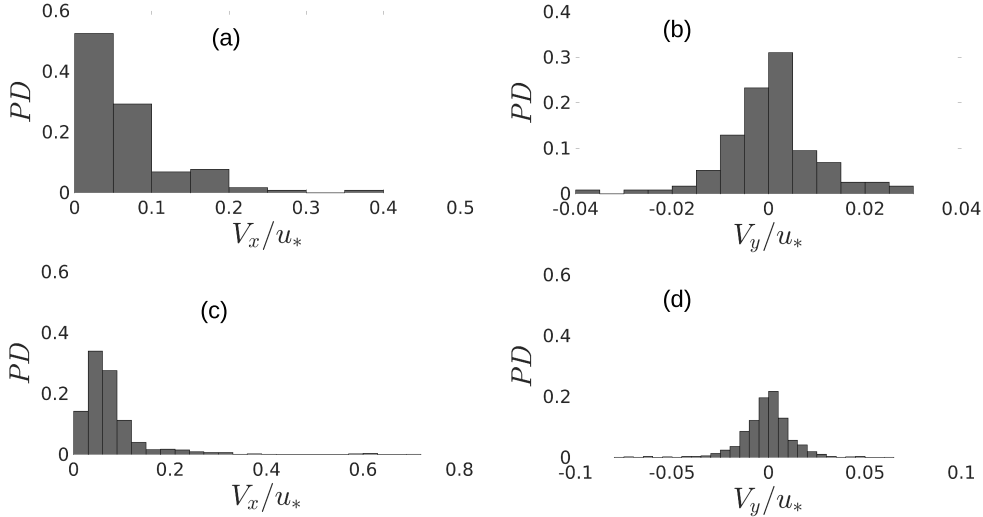


**Figure 14.** PDs of time-averaged velocities in: (a) and (c) the longitudinal direction and (b) and (d) the transverse direction,  $V_x$  and  $V_y$ , respectively, normalized by  $u_*$ . Figures (a) and (b) correspond to the merging and (c) and (d) to the exchange pattern.

601 Finally, we computed the diffusion length  $l_d = \sigma_y^2 / (2\Delta x)$ , where  $\sigma_y$  is the standard  
 602 deviation of the transverse displacement, as proposed by Seizilles et al. (2014) for bed-  
 603 load over a plane bed, though in the present case grains move over a curved bed: they  
 604 follow an upward slope along the symmetry line, with a varying lateral inclination from  
 605 the symmetry line toward the flanks. We found  $l_d/L_{drag} \approx 0.10$  and  $0.20$  (correspond-  
 606 ing to  $l_d/d \approx 0.3$  and  $0.5$ ) for the merging and exchange patterns, respectively. These  
 607 values are one order of magnitude higher than that obtained by Seizilles et al. (2014),  
 608 who found  $l_d/L_{drag} \approx 0.012$  (or  $l_d/d \approx 0.03$ ). We believe that the lateral slope amplify  
 609 the transverse component of the motion in subaqueous bedload, which has an erratic ori-  
 610 gin (Seizilles et al., 2014), improving significantly the transverse diffusion and increas-  
 611 ing  $l_d$  by one order of magnitude. For the upward slope in itself, we believe that it has  
 612 no significant effect on  $l_d$  since the diffusion-like mechanism occurs in the transverse di-  
 613 rection.

#### 614 4 Conclusions

615 We investigated the motion of grains while two barchans interacted with each other  
 616 by performing experiments in a water channel, recording images with high-speed and con-  
 617 ventional cameras, and tracking bedforms and individual grains along images. We found  
 618 typical trajectories of grains during barchan-barchan interactions, from which we deter-  
 619 mined the origin and destination of moving grains, the proportions of grains exchanged  
 620 between barchans and lost by the entire system, the respective mass flow rates, and the  
 621 typical lengths and velocities of grains following different paths. Among our findings, we  
 622 showed that the approximate deficits of granular fluxes in the aligned and off-centered  
 623 configurations reach, respectively, 20 and 30% for the chasing and 60 and 20% for the  
 624 fragmentation-chasing patterns. Therefore, in these patterns the downstream bedforms  
 625 decrease in size, moving faster and avoiding collision with the upstream dune. Interest-  
 626 ingly, we found that during the ejection of a new barchan in the exchange pattern in aligned  
 627 configuration, 20% of grains leaving the baby barchan move toward the parent bedform,  
 628 forming two granular branches that connect both dunes during a given period of time.  
 629 In this particular case, we found that these grains move downstream, whereas in the ex-

change pattern in off-centered configuration there are no grains migrating from the baby barchan toward the parent dune, the same occurring in the fragmentation exchange case (for both aligned and off-centered configurations). In addition, we followed the bedforms after collision took place in the merging and exchange patterns, revealing an initial stage, where the impact barchan is stretched until becoming a longitudinal stripe, and a second stage where the stripe widens slowly. For the second stage, we followed grains originally in the impact barchan and showed that they spread with an erratic trajectory over the target dune, having transverse velocities that scale with the front velocity of the stripe and resembling a diffusion process. For these grains, we found a diffusion length  $l_d$  of the order of  $0.1L_{drag}$ , one order of magnitude higher than that obtained by Seizilles et al. (2014) for subaqueous bedload over plane beds, and we conjecture that the lateral slopes of barchans amplify the transverse component of the erratic motion of grains.

In general, the following insights into the modeling of barchan-barchan interactions are gained from this study: (i) in certain cases, there are different trajectories for grains in the presence of an upstream perturbation (caused by the upstream barchan), with grains not being entrained further downstream from certain horns and/or leaving the target barchan along the lee face (instead of through the horns), for instance; (ii) the knowledge of how grains are exchanged between barchans, at different phases of the interaction patterns; (iii) the identification of a diffusion-like mechanism after collision has taken place, and a corresponding diffusion length. These results represent a step toward understanding the barchan coarsening and division, size selection, and variability of barchanoid shapes found in water, air, and other planetary environments.

## Acknowledgments

W. R. Assis is grateful to FAPESP (grant no. 2019/10239-7), and E. M. Franklin is grateful to FAPESP (grant no. 2018/14981-7) and to CNPq (grant no. 400284/2016-2) for the financial support provided. The authors would like to thank Fernando David Cúñez for the assistance with the image processing code. Data supporting this work are available in the supporting information and in <http://dx.doi.org/10.17632/f9p59sxm4f>.

## References

- Alvarez, C. A., & Franklin, E. M. (2018, Oct). Role of transverse displacements in the formation of subaqueous barchan dunes. *Phys. Rev. Lett.*, *121*, 164503. Retrieved from <https://link.aps.org/doi/10.1103/PhysRevLett.121.164503> doi: 10.1103/PhysRevLett.121.164503
- Alvarez, C. A., & Franklin, E. M. (2019, Oct). Horns of subaqueous barchan dunes: A study at the grain scale. *Phys. Rev. E*, *100*, 042904. Retrieved from <https://link.aps.org/doi/10.1103/PhysRevE.100.042904> doi: 10.1103/PhysRevE.100.042904
- Assis, W. R., & Franklin, E. M. (2020). A comprehensive picture for binary interactions of subaqueous barchans. *Geophys. Res. Lett.*, *47*(18), e2020GL089464.
- Bacik, K. A., Lovett, S., Caulfield, C.-c. P., & Vriend, N. M. (2020, Feb). Wake induced long range repulsion of aqueous dunes. *Phys. Rev. Lett.*, *124*, 054501. Retrieved from <https://link.aps.org/doi/10.1103/PhysRevLett.124.054501> doi: 10.1103/PhysRevLett.124.054501
- Bagnold, R. A. (1941). *The physics of blown sand and desert dunes*. London: Chapman and Hall.
- Bo, T. L., & Zheng, X. J. (2013). Collision behaviors of barchans in aeolian dune fields. *Environ. Earth. Sci.*, *70*, 2963-2970.
- Bristow, N. R., Blois, G., Best, J. L., & Christensen, K. T. (2018). Turbulent flow structure associated with collision between laterally offset, fixed-bed barchan

- 680 dunes. *J. Geophys. Res.-Earth*, *123*(9), 2157-2188.
- 681 Bristow, N. R., Blois, G., Best, J. L., & Christensen, K. T. (2019). Spatial scales  
682 of turbulent flow structures associated with interacting barchan dunes. *J. Geo-*  
683 *phys. Res.-Earth*, *124*(5), 1175-1200.
- 684 Bristow, N. R., Blois, G., Best, J. L., & Christensen, K. T. (2020). Secondary flows  
685 and vortex structure associated with isolated and interacting barchan dunes. *J.*  
686 *Geophys. Res.-Earth*, *125*(2), e2019JF005257.
- 687 Claudin, P., & Andreotti, B. (2006). A scaling law for aeolian dunes on Mars,  
688 Venus, Earth, and for subaqueous ripples. *Earth Plan. Sci. Lett.*, *252*, 20-44.
- 689 Crocker, J. C., & Grier, D. G. (1996). Methods of digital video microscopy for col-  
690 loidal studies. *Journal of Colloid and Interface Science*, *179*(1), 298-310.
- 691 Cúñez, F. D., & Franklin, E. M. (2020). Crystallization and jamming in narrow flu-  
692 idized beds. *Phys. Fluids*, *32*(8), 083303.
- 693 Durán, O., Schwämmle, V., & Herrmann, H. (2005, Aug). Breeding and solitary  
694 wave behavior of dunes. *Phys. Rev. E*, *72*, 021308. Retrieved from [https://](https://link.aps.org/doi/10.1103/PhysRevE.72.021308)  
695 [link.aps.org/doi/10.1103/PhysRevE.72.021308](https://link.aps.org/doi/10.1103/PhysRevE.72.021308) doi: 10.1103/PhysRevE  
696 .72.021308
- 697 Durán, O., Schwämmle, V., Lind, P. G., & Herrmann, H. (2009). The dune size dis-  
698 tribution and scaling relations of barchan dune fields. *Granular Matter*, *11*, 7-  
699 11.
- 700 Elbelrhiti, H., Andreotti, B., & Claudin, P. (2008). Barchan dune corridors: Field  
701 characterization and investigation of control parameters. *Journal of Geophysic-*  
702 *al Research: Earth Surface*, *113*(F2).
- 703 Elbelrhiti, H., Claudin, P., & Andreotti, B. (2005). Field evidence for surface-wave-  
704 induced instability of sand dunes. *Nature*, *437*(04058).
- 705 Endo, N., Taniguchi, K., & Katsuki, A. (2004). Observation of the whole process  
706 of interaction between barchans by flume experiments. *Geophys. Res. Lett.*,  
707 *31*(12).
- 708 Fischer, S., Cates, M. E., & Kroy, K. (2008, Mar). Dynamic scaling of desert dunes.  
709 *Phys. Rev. E*, *77*, 031302. Retrieved from [https://link.aps.org/doi/](https://link.aps.org/doi/10.1103/PhysRevE.77.031302)  
710 [10.1103/PhysRevE.77.031302](https://link.aps.org/doi/10.1103/PhysRevE.77.031302) doi: 10.1103/PhysRevE.77.031302
- 711 Gay, S. P. (1999). Observations regarding the movement of barchan sand dunes in  
712 the nazca to tanaca area of southern peru. *Geomorphology*, *27*(3), 279 - 293.
- 713 Génois, M., du Pont, S. C., Hersen, P., & Grégoire, G. (2013). An agent-based  
714 model of dune interactions produces the emergence of patterns in deserts. *Geo-*  
715 *phys. Res. Lett.*, *40*(15), 3909-3914.
- 716 Génois, M., Hersen, P., du Pont, S., & Grégoire, G. (2013). Spatial structuring  
717 and size selection as collective behaviours in an agent-based model for barchan  
718 fields. *Eur. Phys. J. B*, *86*(447).
- 719 Herrmann, H. J., & Sauermann, G. (2000). The shape of dunes. *Physica A (Amster-*  
720 *dam)*, *283*, 24-30.
- 721 Hersen, P. (2004). On the crescentic shape of barchan dunes. *Eur. Phys. J. B*,  
722 *37*(4), 507-514.
- 723 Hersen, P., Andersen, K. H., Elbelrhiti, H., Andreotti, B., Claudin, P., & Douady,  
724 S. (2004, Jan). Corridors of barchan dunes: Stability and size selection. *Phys.*  
725 *Rev. E*, *69*, 011304. Retrieved from [https://link.aps.org/doi/10.1103/](https://link.aps.org/doi/10.1103/PhysRevE.69.011304)  
726 [PhysRevE.69.011304](https://link.aps.org/doi/10.1103/PhysRevE.69.011304) doi: 10.1103/PhysRevE.69.011304
- 727 Hersen, P., & Douady, S. (2005). Collision of barchan dunes as a mechanism of size  
728 regulation. *Geophys. Res. Lett.*, *32*(21).
- 729 Hersen, P., Douady, S., & Andreotti, B. (2002, Dec). Relevant length  
730 scale of barchan dunes. *Phys. Rev. Lett.*, *89*, 264301. Retrieved from  
731 <https://link.aps.org/doi/10.1103/PhysRevLett.89.264301> doi:  
732 [10.1103/PhysRevLett.89.264301](https://link.aps.org/doi/10.1103/PhysRevLett.89.264301)
- 733 Houssais, M., Ortiz, C. P., Durian, D. J., & Jerolmack, D. J. (2015). Onset of sed-  
734 iment transport is a continuous transition driven by fluid shear and granular

- 735 creep. *Nat. Commun.*, *6*(6527).
- 736 Hugenholtz, C. H., & Barchyn, T. E. (2012). Real barchan dune collisions and ejections. *Geophys. Res. Lett.*, *39*(2).
- 737
- 738 Katsuki, A., Kikuchi, M., Nishimori, H., Endo, N., & Taniguchi, K. (2011). Cellular
- 739 model for sand dunes with saltation, avalanche and strong erosion: collisional
- 740 simulation of barchans. *Earth Surf. Process. Landforms*, *36*(3), 372-382.
- 741 Katsuki, A., Nishimori, H., Endo, N., & Taniguchi, K. (2005). Collision dynamics of
- 742 two barchan dunes simulated using a simple model. *J. Phys. Soc. Jpn.*, *74*(2),
- 743 538-541.
- 744 Kelley, D. H., & Ouellette, N. T. (2011). Using particle tracking to measure flow
- 745 instabilities in an undergraduate laboratory experiment. *Am. J. Phys.*, *79*(3),
- 746 267-273.
- 747 Kocurek, G., Ewing, R. C., & Mohrig, D. (2010). How do bedform patterns arise?
- 748 new views on the role of bedform interactions within a set of boundary condi-
- 749 tions. *Earth Surf. Process. Landforms*, *35*(1), 51-63.
- 750 Kroy, K., Sauermann, G., & Herrmann, H. J. (2002a, Sep). Minimal model for aeolian
- 751 sand dunes. *Phys. Rev. E*, *66*, 031302. Retrieved from [https://link.aps](https://link.aps.org/doi/10.1103/PhysRevE.66.031302)
- 752 [.org/doi/10.1103/PhysRevE.66.031302](https://link.aps.org/doi/10.1103/PhysRevE.66.031302) doi: 10.1103/PhysRevE.66.031302
- 753 Kroy, K., Sauermann, G., & Herrmann, H. J. (2002b, Jan). Minimal model for sand
- 754 dunes. *Phys. Rev. Lett.*, *88*, 054301. Retrieved from [https://link.aps.org/](https://link.aps.org/doi/10.1103/PhysRevLett.88.054301)
- 755 [doi/10.1103/PhysRevLett.88.054301](https://link.aps.org/doi/10.1103/PhysRevLett.88.054301) doi: 10.1103/PhysRevLett.88.054301
- 756 Lima, A., Sauermann, G., Herrmann, H., & Kroy, K. (2002). Modelling a dune field.
- 757 *Physica A*, *310*(3), 487-500. Retrieved from [https://www.sciencedirect](https://www.sciencedirect.com/science/article/pii/S0378437102005460)
- 758 [.com/science/article/pii/S0378437102005460](https://www.sciencedirect.com/science/article/pii/S0378437102005460)
- 759 Norris, R. M., & Norris, K. S. (1961). Algodones Dunes of Southeastern California.
- 760 *GSA Bulletin*, *72*(4), 605-619.
- 761 Pähitz, T., Kok, J. F., Parteli, E. J. R., & Herrmann, H. J. (2013). Flux saturation
- 762 length of sediment transport. *Phys. Rev. Lett.*, *111*, 218002.
- 763 Palmer, J. A., Mejia-Alvarez, R., Best, J. L., & Christensen, K. T. (2012). Particle-
- 764 image velocimetry measurements of flow over interacting barchan dunes. *Exp.*
- 765 *Fluids*, *52*, 809-829.
- 766 Parteli, E., & Herrmann, H. (2003). A simple model for a transverse dune field.
- 767 *Physica A*, *327*(3), 554-562.
- 768 Parteli, E. J. R., & Herrmann, H. J. (2007, Oct). Dune formation on the present
- 769 mars. *Phys. Rev. E*, *76*, 041307. Retrieved from [https://link.aps.org/doi/](https://link.aps.org/doi/10.1103/PhysRevE.76.041307)
- 770 [10.1103/PhysRevE.76.041307](https://link.aps.org/doi/10.1103/PhysRevE.76.041307) doi: 10.1103/PhysRevE.76.041307
- 771 Schlichting, H. (2000). *Boundary-layer theory*. New York: Springer.
- 772 Schwämmle, V., & Herrmann, H. J. (2003). Solitary wave behaviour of sand dunes.
- 773 *Nature*, *426*, 619-620.
- 774 Seizilles, G., Lajeunesse, E., Devauchelle, O., & Bak, M. (2014). Cross-stream diffu-
- 775 sion in bedload transport. *Phys. Fluids*, *26*(1), 013302.
- 776 Vermeesch, P. (2011). Solitary wave behavior in sand dunes observed from space.
- 777 *Geophys. Res. Lett.*, *38*(22).
- 778 Worman, S. L., Murray, A. B., Littlewood, R., Andreotti, B., & Claudin, P. (2013,
- 779 10). Modeling emergent large-scale structures of barchan dune fields. *Geology*,
- 780 *41*(10), 1059-1062.
- 781 Zheng, X. J., Bo, T. L., & Zhu, W. (2009). A scale-coupled method for simulation
- 782 of the formation and evolution of aeolian dune field. *Int. J. Nonlinear Sci. Numer. Simul.*, *10*(3), 387-396.
- 783
- 784 Zhou, X., Wang, Y., & Yang, B. (2019). Three-dimensional numerical simulations of
- 785 barchan dune interactions in unidirectional flow. *Particul. Sci. Technol.*, *37*(7),
- 786 835-842.